J. Fluid Mech. (1970), *vol.* 44, *part* 1, *pp.* 79–95
Printed in Great Britain

Characteristics of Ekman boundary layer instabilities

By D. R. CALDWELL
Department of Oceanography, Oregon State University
AND C. W. VAN ATTA
Scripps Institution of Oceanography, University of California at San Diego

(Received 20 December 1969)

In a laboratory study, the class of instabilities of the laminar Ekman layer called type II (or class A) are found to have the spectral characteristics of narrow-band noise ($Q \sim 5$). The unperturbed laminar profile resembles very closely the ideal Ekman solution. The frequency of the spectral peak varies with the Reynolds number as predicted theoretically by Lilly (1966), but the measured frequencies are only 60 % of the predicted value. The critical Reynolds number for this instability is found to be 56·7, in good agreement with Lilly's analysis. The measured boundary layer profile of the magnitude of the spectral peak has the behaviour predicted by Lilly. A sudden onset of turbulence is found at a Reynolds number of 148.

1. Introduction

The instabilities of the Ekman layer have been studied experimentally by Faller (1963), by Faller & Kaylor (1966), and by Tatro & Mollo-Christensen (1967). Theoretical investigations have been carried out by Lilly (1966) and by Faller & Kaylor (1965, 1966). Using flow visualization techniques, Faller made the first observations of 'waves' forming in an Ekman flow, at Reynolds numbers above 125. (The Reynolds number Re is defined as VD/ν where V is the speed of flow outside the boundary layer, D the boundary layer depth, and ν the kinematic viscosity.) Faller & Kaylor (1965) described another type of wave found at $Re > 70$. Tatro & Mollo-Christensen studied these waves in more detail using hot-wire anemometers and found both waves, at slightly different critical Reynolds numbers. Turbulence appeared at Reynolds numbers above 200. In these papers, the instability which starts at lower Reynolds numbers is called type II, and the one at higher Reynolds numbers is called type I. In Greenspan's (1968) review, type II is called class A and type I is called class B. Lilly, and Faller & Kaylor, used numerical techniques to study the problem, and obtained values for the critical Reynolds numbers and some parameters of the waves. It should be noted that the rotation rate is assumed to be very large, i.e. the Rossby number is assumed to be zero, in the theoretical studies. A compilation of the results of experiment and theory is given in table 1.

The identification of the type I and II waves seen in the experiment with the instabilities found by Lilly seems well established, although there has been no

detailed study of the wave forms or spectra of these waves. The question of how well the ideal Ekman flow is realized in these earlier experiments is not known: Faller made no measurements of boundary layer profiles, and Tatro & Mollo-Christensen found that the thickness of the boundary layer in laminar flow varied with position and Reynolds number (in the ideal Ekman flow boundary layer thickness depends only on the rotation rate and the kinematic viscosity of the fluid). They presented no comparison of individual measured and theoretical profiles, however. No one actually measured a velocity profile. There is some

		Theory		Experiment		
Type of instability	Quantity	Faller & Kaylor	Lilly	Faller, Faller & Kaylor	Tatro *et al.*	Present work
Type II (class A)	Critical Reynolds number	55	55	< 70	56·3 + 116·8 *Ro*	56·7
	Wavelength, in Ekman depths	24	21	22 to 33	27·8 ± 2·0	(Frequency 61% of that predicted by Lilly)
	ϵ†	−15°	−20°	+5° to −20°	0 to −8°	
	Velocity divided by geostrophic	0·50	0·57	—	0·16	
Type I (class B)	Critical Reynolds number	118	110	125 ± 5	124·5 + 7·32*Ro*	—
	Wavelength, in Ekman depths	11	11·9	10·9	11·8	—
	ϵ†	10°–12°	8°	+14·5 ± 2·0°	+14·8° ± 0·8°	—
	Velocity divided by geostrophic	0·33(11°)	0·094	0·023(14·5°)	0·034	—

ϵ† is the angle between wavefront and geostrophic wind.

TABLE 1. Summary of Ekman layer instabilities

question as to whether the critical Reynolds number for type II (class A) waves depends on Rossby number: Tatro & Mollo-Christensen found that it did, but Faller (1966) suggests that it does not. For some of the parameters of the waves, there are discrepancies between Lilly's results and the measurements; for example, Tatro & Mollo-Christensen found the phase speed for the type II waves to be less than $\frac{1}{3}$ of the phase speed predicted, although the discrepancy in wavelength was only 30%. Using an apparatus similar to that of Tatro & Mollo-Christensen, we sought to clear up some of these points, and then study the transition to turbulence, which has not been pursued in the previous studies. Using digital recording and data-processing techniques made it practical, in terms of time and effort, to examine the resulting spectra, which contained fairly discrete waves and turbulence simultaneously. As will be explained below, we can distinguish the type II (class A) waves and the turbulence in the spectra, but we saw no type I (class B) waves.

2. Apparatus

A schematic of the flow system, which is mounted on a rotating table, is given in figure 1. Air is drawn in on top of the table, brought to the outside under plate C, made to flow to the centre between plates A and B, and then blown out up the centre pipe. The mass flow was monitored by a Pitot-static tube placed in the blower outlet. The table was rotated by a Graham variable speed transmission at speeds continuously variable up to 105 rev/min. The transmission is powered by a three-phase motor which holds the table speed as steady as the power line frequency.

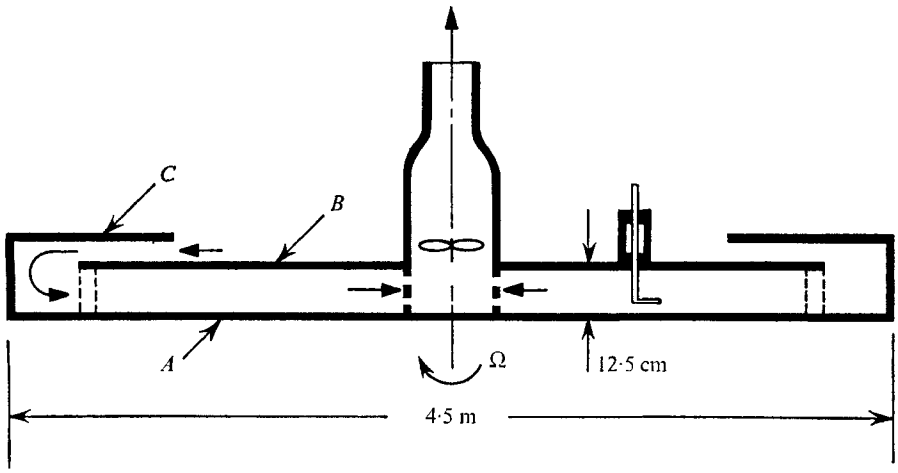

FIGURE 1. Schematic diagram of rotating apparatus.

Measurements of mean and fluctuating velocities were made near the bottom surface of plate B, near the top surface of plate A, and in the interior flow between the plates using four types of hot-wire probes as shown in figure 2. These probes, which were inserted through one of a series of holes drilled in plate B, were used as follows:

(i) This probe placed the hot wire, aligned vertically, at the midpoint between plates A and B for measurements of the magnitude of the velocity in the interior of the flow.

(ii) This probe, when used with the traverse described below, placed the hot wire, horizontally aligned, in the boundary layer near the lower plate. When the 'bottom detector,' the small rod at the bend near the bottom, touched plate A, a relay circuit stopped the vertical drive motor on the traverse, allowing placement of the hot wire very close to plate A without damage.

(iii) This probe, used with the traverse, could be rotated to place a vertical hot wire at different radii, midway between the plates. This allowed measurement of the interior flow at continuously variable radii, which is not possible with probes such as (i).

(iv) This wire was mounted on a lucite plug machined to fit flush with the bottom of plate B.

A remotely controlled traverse was used to adjust the vertical position and orientation of probes (i), (ii) and (iii). The degree of rotation was indicated by a

potentiometer. Vertical displacements were measured by pulses from a microswitch triggered by a cam mounted on the shaft which moved the probe. Each revolution of this shaft corresponded to 0·0025 in. of vertical motion.

Electrical connections to the rotating apparatus were provided by two sets of slip rings. A set of copper strips dipped in mercury-filled grooves was used for both high power and low noise circuits. A set of mechanical rings was used for less critical circuits.

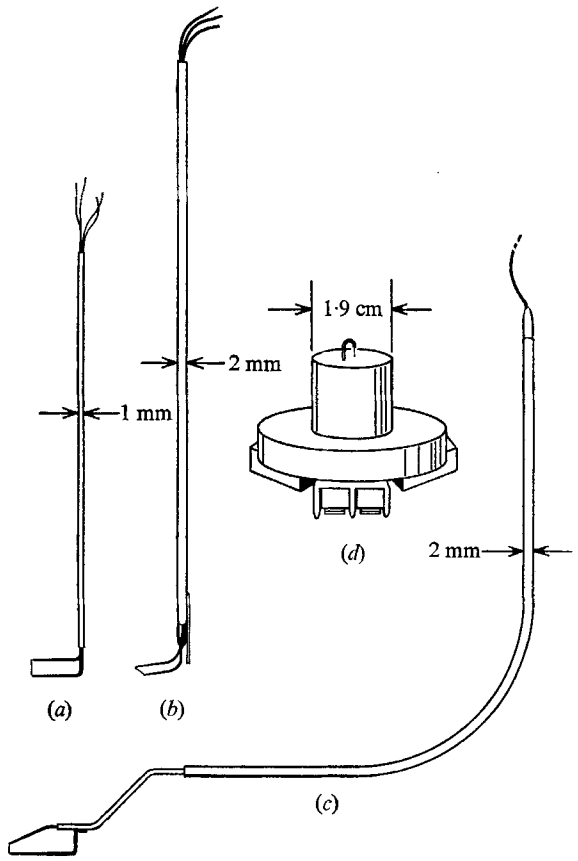

FIGURE 2. Hot-wire probes.

The hot-wire measurements were made in two ways. For mean flow measurements, the hot wire was connected to a constant resistance circuit (DISA Model 55A01). The voltage required to keep the hot wire at constant resistance was measured by a voltage-to-frequency converter and a counter. Some of the turbulence measurements were made by high passing and recording this signal. Some of the measurements of low-frequency fluctuations were made by operating the wire in the constant current mode, where the hot wire was connected in series with two 12 V car batteries and a 1000 ohm resistor for a 'constant current' mode of operation. The voltage across the hot wire was amplified and band-passed (band 0·1 to 20 c/s) before the signal was passed through the slip rings. Signals were recorded digitally on a system composed of a Vidar scanner, Preston amplifier, Applied Development Corporation analog-to-digital converter

and an incremental tape recorder. The recorder can make 500 steps per sec, so with twelve-bit accuracy and one channel, for example, 250 numbers per sec can be recorded.

3. The basic interior flow

For the initial experiments the apparatus was smaller than shown in figure 1. The plate separation was the same, but the overall diameter was only 214 cm (measured to the last entrance screen). The interior flow was measured with probes (i) and (ii). Probe (iii) was used to determine the direction of flow. The flow direction was found to be nearly tangential, with the flow spiralling in at an angle of one or two degrees from tangential, depending on the speed of flow and the rate of rotation.

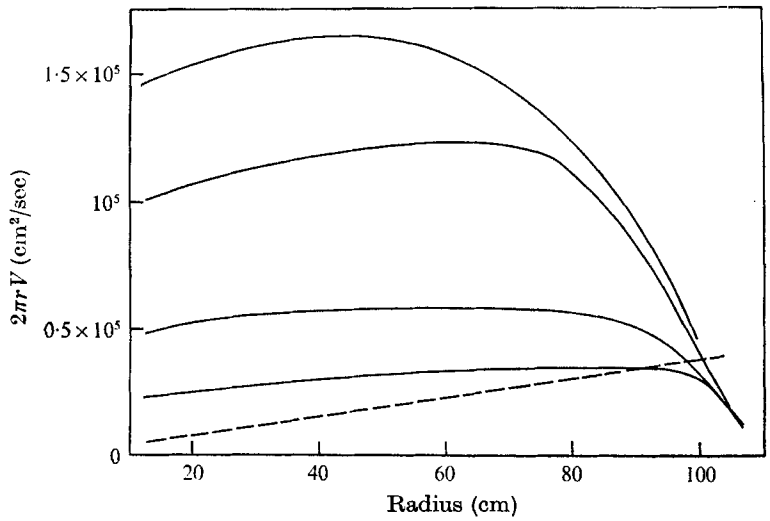

FIGURE 3. The circulation, $2\pi Vr$, as a function of r, for four different flow rates. The last entering screen was at $r = 108$ cm. The rotation period was 2·50 sec. The dashed line represents the circulation at each radius for which the Reynolds number would be 100.

Figure 3 shows the circulation, $2\pi Vr$, as a function of r, the radius. If the Rossby number $Ro\,(= V/2\pi\Omega$, where Ω is the basic rotation rate) were zero, and the flow of infinite horizontal extent, the circulation should be the same everywhere. (It should be noted that V is the speed of circumferential flow relative to the rotating plates.) The direction of flow in the core would be exactly tangential with transport to the centre occurring only in the boundary layer on each plate. The circulation would be equal to S/D, where S is the volume flow through the blower and $D = (\nu/\Omega)^{\frac{1}{2}}$, the Ekman layer depth. Near the boundaries the flow would be described by

$$u = [\sin(z/D)\exp(-z/D)]S/(2\pi Dr),$$

$$v = [1-\cos(z/D)\exp(-z/D)]S/(2\pi Dr),$$

where u is the radial component and v the tangential component of velocity and z is the vertical distance from the boundary. As $z\to\infty$, $u\to 0$ and $v\to V$.

This flow, which satisfies the equation of continuity exactly, and satisfies the Navier–Stokes equation in the limit of zero Rossby number, is an ideal Ekman layer bounding an exactly geostrophic core flow. This flow will not be realized in the present apparatus because: (i) the flow is not horizontally infinite, but must develop from the outer edge of the plates, and (ii) the Rossby number cannot be made small enough. Figure 4 shows the effect of both development and non-zero Rossby number on the circulation. Near the outer edge of the table the circulation (calculated in the rotating system) is very low. It increases as the flow develops inward and then decreases as the Rossby number becomes even larger near the centre of the table. Figure 4 shows the behaviour in the outer region in

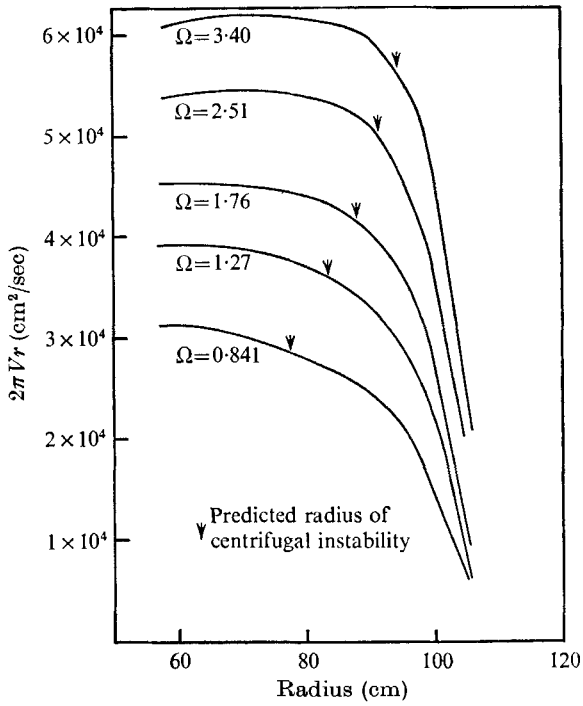

FIGURE 4. The circulation, $2\pi Vr$, as a function of radius with rotation rate as a parameter, near the outer radius. The arrows indicate the estimated radius for centrifugal instability.

detail at different rotation rates. At the lower rotation rates the outer adjustment region extends farther toward the centre. Centrifugal instability seems to be the cause of this long adjustment region. The circulation of the flow in the rotating co-ordinate system at the radius r is $2\pi r V(r)$. In the stationary system it is $2\pi r V(r) + 2\pi r\Omega^2 = S/D + 2\pi r\Omega^2$. At the outer screen, $r = R$, the fluid has not yet been accelerated faster than the basic rotation so its circulation is at most $2\pi R\Omega^2$. There must, therefore, be a region where $V(r)$ is such that the circulation decreases as we go outward. But centrifugal stability would require the circulation to increase outward, so this region must be unstable. The inner boundary of this region might be predicted by setting $2\pi r V(r) = 2\pi R\Omega^2$. This equation can be solved for the value of r at which the circulation becomes equal to the circulation

at the rim. On figure 4, this predicted radius has been marked with an arrow for each value of Ω. In the adjustment region, the hot-wire signal shows very large oscillations indicating large eddies in the flow.

Because of the wide region of adjustment, we decided to increase the size of the apparatus so the eddies would not interfere with measurements. The radius of the last screen was increased from 107 cm to 190·5 cm. Now, the inside edge of the adjustment zone should be at $r = 183$ cm for $Vr = 10^4$ cm^2/sec, $\Omega = 2{\cdot}5$ radians/sec, instead of 95 cm. Figure 5 shows the circulation before and after this change.

The circulation drops smoothly with decreasing radius, probably because of non-linear effects associated with the increasing Rossby number, but the velocity continually increases inward to the smallest radius studied, only 0·5 cm from the inside screen.

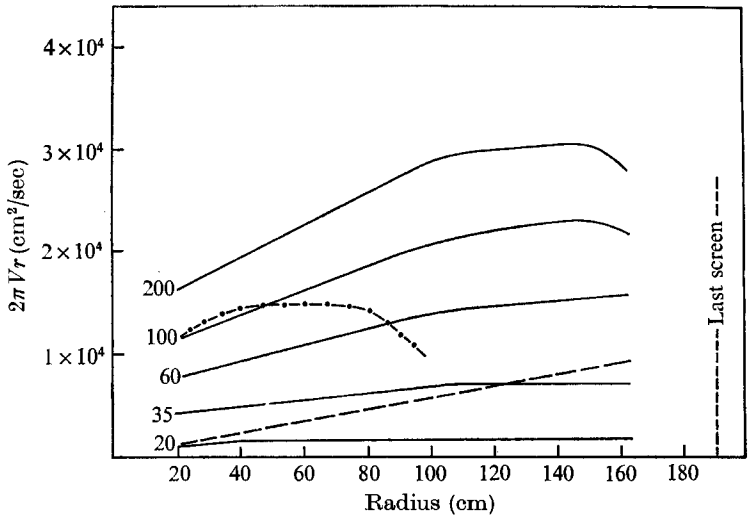

FIGURE 5. The circulation, $2\pi Vr$, as a function or radius for the rebuilt (larger) apparatus, for five different flow rates. The rotation period was 1·00 sec. The dashed line represents the circulation at each radius for which the Reynolds number would be 100. The dotted and dashed line is the circulation in the old (smaller) apparatus for one flow rate. –·–, smaller table.

4. Boundary layer mean flow profiles

An example of the measured laminar boundary layer flow profiles is shown as figure 6. The data were taken with probe (ii) (see figure 2). At a given height, the probe was rotated and the response as a function of direction plotted. The direction of maximum apparent speed was found, and the speed measured at that angle. The zero angle is taken as the direction of flow well away from the plate. Measurements could not be made closer than about 0·02 cm from the plate, because of heat losses from the hot wire to the plate. The measured boundary layer thickness δ was defined as the height z where $v/V = 0{\cdot}8$, which corresponds to $z = D$ in the Ekman solution. For most of the measurements, the v component alone was determined by aligning the hot wire parallel to the radius for the entire

traverse. Close agreement between the measured profiles and the Ekman solution is clearly seen in figure 6.

In order to investigate the variation of δ with radius, δ was measured at several blower speeds (below wave-producing speeds) at several radii. The results are shown in table 2. There is little variation of boundary layer thickness with either speed of flow or radius at these low Reynolds numbers. In view of this result, it is not clear why Tatro & Mollo-Christensen did observe a significant radial variation.

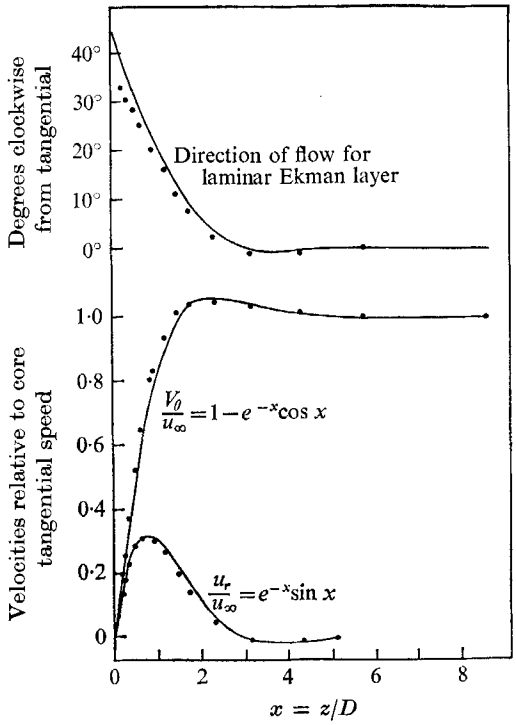

FIGURE 6. Velocity profiles for the laminar boundary layer. The rotation period is 2·50 sec, Reynolds number 103, Rossby number 0·125 and radius 97 cm.

Radius	Reynolds number	Rossby number	$\delta/(\nu/\Omega)^{\frac{1}{2}}$
97 cm	33	0·039	0·997
	50	0·0595	0·965
	64	0·076	0·988
	78	0·092	1·000
	90	0·107	0·965
	108	0·128	1·010
	123	0·146	1·035
36 cm	52	0·166	1·014
	92·5	0·296	1·028
	131	0·418	1·008

TABLE 2. Measurements of the depth δ of the laminar Ekman layer

At higher Reynolds numbers the boundary layer profile and thickness change radically with increasing Reynolds number. Turbulence smooths out the profiles and eliminates the overshoot as shown in figure 7.

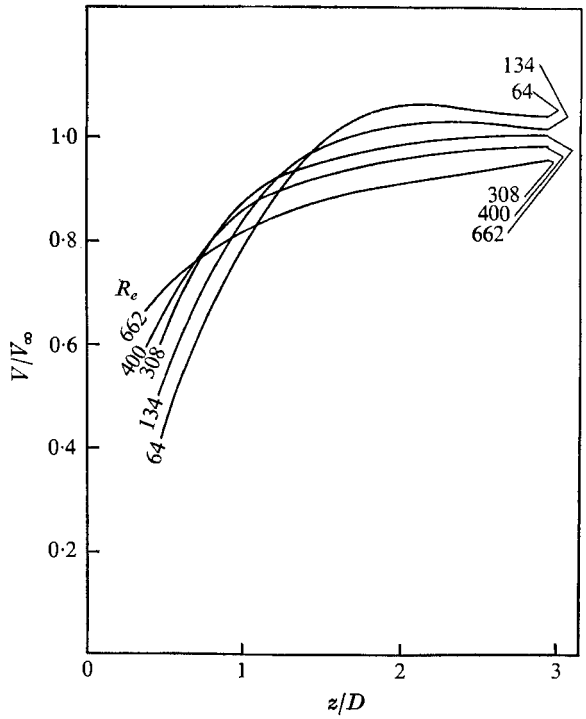

FIGURE 7. Tangential velocity profiles at various Reynolds numbers. The rotation period was 1·62 sec, radius 82 cm. The Rossby number for each profile is equal to the Reynolds number divided by 855.

5. Onset of instability

The hot-wire signal began to exhibit a wavelike character as the Reynolds number was increased. Characteristic records are shown in figures 8 and 9. As the Reynolds number was slowly increased, the waves appeared quite suddenly. The amplitude at first increased rapidly with increasing Reynolds number and then grew more slowly. With further increase in Reynolds number, the waves eventually were submerged in the turbulent signal.

The critical Reynolds number was found by observing the waves on an oscilloscope to find their approximate frequency, then feeding the signal from the hot-wire through a Krohn–Hite band pass filter with both cut-off frequencies set at the wave frequency. The filtered wave signal was then fed to a Hewlett–Packard voltage-to-frequency converter, which gives a pulse rate proportional to the magnitude of its input voltage, regardless of polarity. The pulse rate was averaged by a counter for typically 100 sec. The output of the counter was plotted against Reynolds number until a sudden increase in reading showed that the waves started. A typical plot is shown in figure 10. Critical Reynolds numbers measured

in this way corresponded exactly with those taken from complete spectral analyses.

The critical Reynolds number for the observed waves seems to depend on

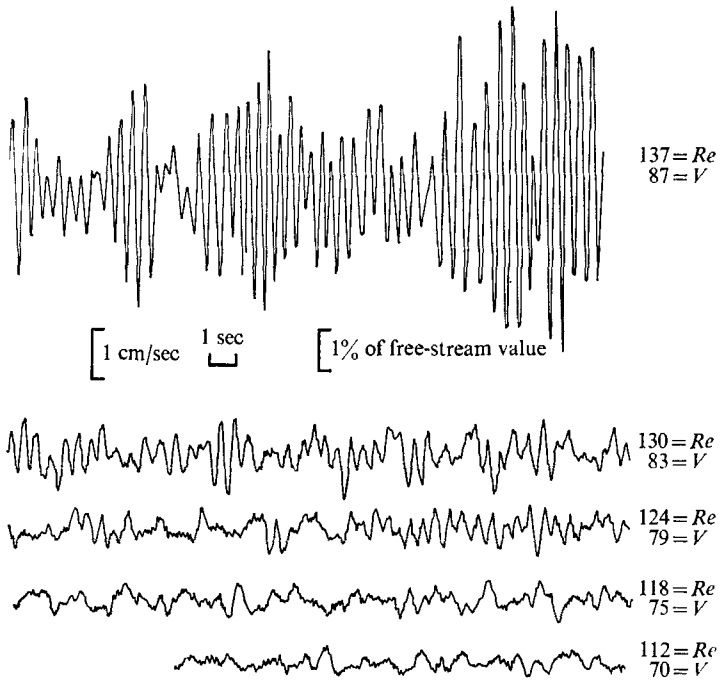

FIGURE 8. Chart recordings of the waves near onset. The signal was low-passed at 20 c/s. The apparent critical Reynolds number for this Rossby number ($\sim$ 0·14) is 120. The rotation period was 3·32 sec, the radius 97 cm.

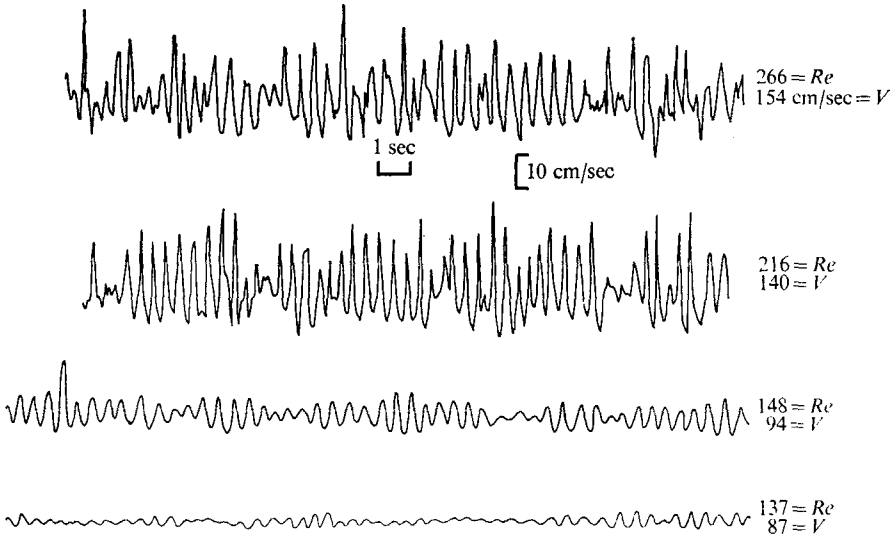

FIGURE 9. Chart recordings of the waves at higher Reynolds numbers, for the same conditions as figure 8 (but greatly compressed vertical scale). The record for Re = 137 is repeated for comparison.

Rossby number, or at least on the radius at which the observation is made. Figure 11 shows the critical Reynolds number as a function of Rossby number. Tatro & Mollo-Christensen found an apparent radial dependence, which was removed when the measured boundary layer thickness and tangential velocity were used in calculating the Reynolds number, instead of using D and a velocity based solely on the total mass flow. Our critical Reynolds numbers which were computed using the measured tangential velocity and the measurements of

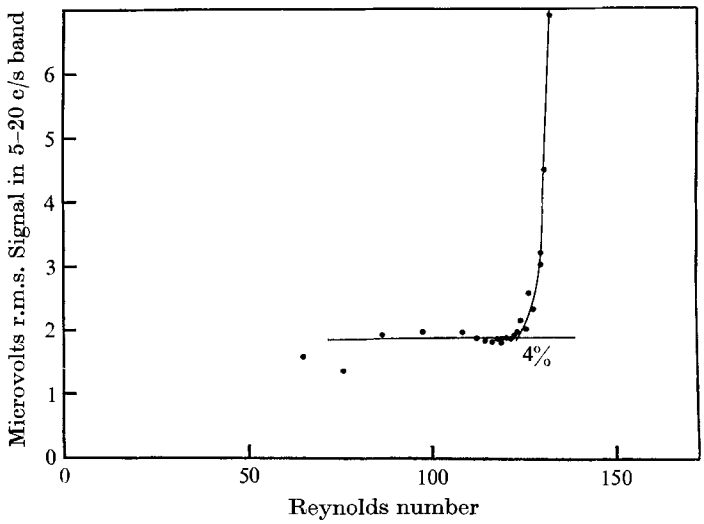

FIGURE 10. Power from constant current hot wire after filtering with band pass filter with both cut-off frequencies set on the peak wave frequency.

boundary layer depth shown in table 2 (which shows no measurable deviation from $D = (\nu/\Omega^{\frac{1}{2}})$), still exhibit an apparent variation of critical Reynolds number with either radius or Rossby number. This is explainable by a remark of Faller & Kaylor (1966, p. 479), that apparent variations of critical Reynolds number with Rossby number in the present type of apparatus might be due to the fact that as the disturbances grow from infinitesimal amplitude they move into regions of higher Reynolds number. The apparent critical Reynolds number, then, will always be higher than the Reynolds number at which they started to grow. The increase will depend on the Rossby number, according to the expression given by Faller

$$Re^2(Re - Re_c)\,(Re^{-2} - Re_c^{-2}) = \frac{2c_r}{a}\,.\,Ro\,.\log_e(A/Ac),$$

where

Re = apparent critical Reynolds number,

Re_c = true critical Reynolds number,

Ro = Rossby number,

c_r = phase speed divided by external velocity,

a = growth rate of waves divided by Ω,

A = minimum detectable amplitude,

A_c = amplitude of waves when they start to grow.

When the data shown in figure 11 is fitted to this relationship in a least squares sense, we find the best fit with $Re_c = 56{\cdot}7 \pm 3$ and $A/A_c \cong 5 \times 10^4$. This value of Re_c agrees very closely with that calculated by Lilly and observed by Tatro & Mollo-Christensen (see table 1). It might be noted that the determinations of critical Reynolds number were made by increasing the blower speed with rotation rate constant until the waves appeared. This procedure increases the Reynolds number and Rossby number proportionately, so we approached the curve of apparent critical Reynolds number *vs.* Rossby number at an oblique angle. This may be the cause of much of the scatter in the points in figure 11.

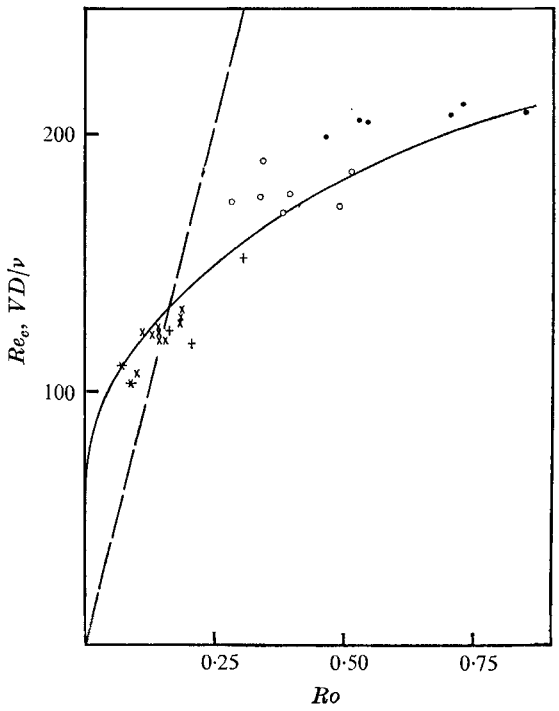

FIGURE 11. Critical Reynolds number *vs.* Rossby number. The symbols represent different radii. (●, 35·9 cm; ○, 51·1 cm; +, 66·4 cm; ×, 97 cm; and ⁎, 132·4 cm). The solid line is Faller's formula, $Re^2(Re - Re_c)(Re_c^{-2} - Re^{-2}) = CRo$ where $Re_c = 56{\cdot}7 \pm 3$ and C are determined by a least squares fit to the data shown. The dashed line is the locus in the diagram for $r = 97$ cm and $\Omega = 2{\cdot}5$ rad/sec. This line is the path taken in a run.

It seems, then, that we are seeing type II waves. One wonders why we do not see type I waves. A. J. Faller, in the course of reviewing this paper, made the following suggestions: (i) 'If stationary type I bands were present, they would not pass by the hot wire, and there would be no evidence of their existence'. If the phase speed is low, they might pass the hot wire at a frequency comparable to the table rotation rate. At this frequency, the noise level might obscure them. (ii) It is possible that the apparent onset of turbulence near $Re = 148$ might be related to the appearance of type I waves and their interaction with type II waves.

6. Spectra of waves

Spectra were calculated from the hot-wire signals by processing the recordings made as described previously on a Control Data 3600 Computer. The technique used to compute the transform is described by Haubrich (1965), except that the Cooley–Tukey algorithm was used to shorten the computations.

The spectrum changes radically in the Reynolds number range 100 to 200. Figure 12 shows the effect on the spectrum of increasing the Reynolds number from 124, just at onset, to 320. At $Re = 320$, the waves no longer stand out from the general turbulent spectrum, which seems to have an onset point of its own. Figure 13 shows the variation with Reynolds number of the peak energy (energy in a band centred around the spectral maximum) in db and the energy at 6·5 c/s. The waves start first, and stand out well above the noise until $Re \simeq 300$, when they appear to lose energy to the turbulence.

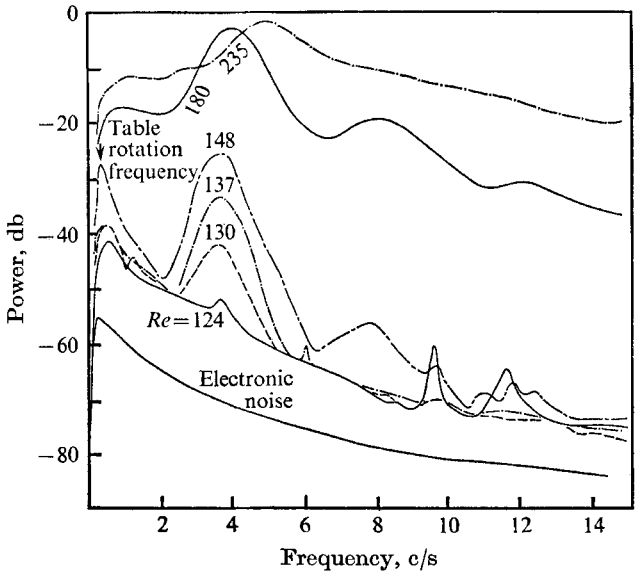

FIGURE 12. Smoothed spectra of signal from a short (0·1 cm) vertical hot wire located about 0·1 cm from the boundary. The lower line is the spectrum of the signal when a resistor is substituted for the hot wire. 16,384 data points were used in analysing the signal into 1024 frequencies so there are 32 degrees of freedom and the elementary frequency band is 0·0152 c/s wide. The Rossby numbers for the spectra are as follows: $Re = 124$, $Ro = 0{\cdot}31$; $Re = 130$, $Ro = 0{\cdot}32$; $Re = 137$, $Ro = 0{\cdot}33$; $Re = 148$, $Ro = 0{\cdot}35$; $Re = 180$, $Ro = 0{\cdot}42$; $Re = 235$, $Ro = 0{\cdot}56$.

Figure 14 shows the relative energy in the waves as a function of distance from the boundary. The shape of the curve, especially the sharp minimum between three and four Ekman depths, compares fairly well with figure 12 of Lilly's paper. We find a minimum in wave energy at $z/D = 3{\cdot}5$: Lilly predicts a minimum at $z/D = 2{\cdot}9$. We found this sharp minimum in every one of the four traverses. The sharpness of this minimum is remarkable for two reasons: (i) the computations do

not show such sharpness and (ii) at this Reynolds number (205), turbulent interactions might be expected to smear out vertical variations.

The peak widths in figure 12 are typical. The Q of the peak is always 4 to 5. The centre frequency, f_0, seems to increase with Reynolds numbers, but not sharply. The quantity $\sigma = 2\pi f_0/\Omega$ should be dependent only on the Reynolds number $(2\pi f_0/\Omega = (2\pi/\Omega)(C_r Vk/2\pi D) = C_r KRe$; C_r is the dimensionless phase speed used by Lilly), so σ is plotted *vs.* Reynolds number in figure 15. Values of frequencies for type I and type II waves as predicted by Lilly are plotted for comparison. Correlation of observed spectra, particularly peak frequencies

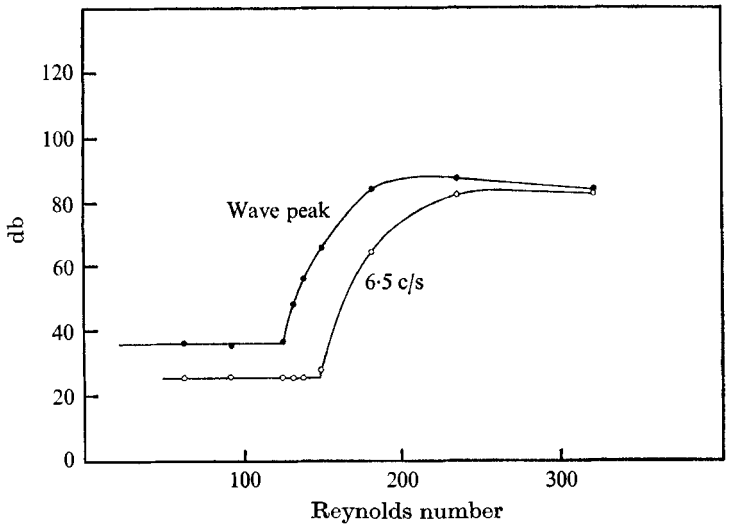

FIGURE 13. Energy near the wave peak, and in a somewhat higher frequency band *vs.* Reynolds number for the runs whose spectra are shown in figure 12.

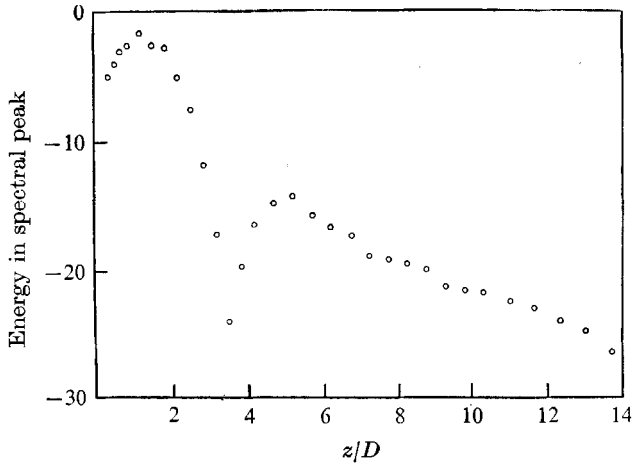

FIGURE 14. Energy contained in the wave peak (band of frequencies 5·31 to 6·53 sec) *vs.* distance from boundary in Ekman depths for r = 81·6 cm, rotation period = 1·63 sec, Rossby number = 0·242. Vertical scale is in db below arbitrary level. Ω = 3·85 rad/sec; Re = 205; f_0 = 5·92 c/s.

(such as are shown in figure 1), with growth rate diagrams like Lilly's (his figures 1 through 8) is very difficult because: (i) The oscillations at a given frequency are produced by waves which have many different values of vector wave-number. Figure 16 shows a diagram similar to Lilly's figure 7 with contours of constant dimensionless frequency σ. The lines of constant frequency cross the contours of growth rate in such a way that, for example, $\sigma = 10$ for waves close to both of the two maxima of growth rate. (ii) The waves are observed at Reynolds numbers much above Re_c; they have grown by a factor of about 50,000, so one cannot expect a linear perturbation calculation to be applicable. (iii) Even if the analysis

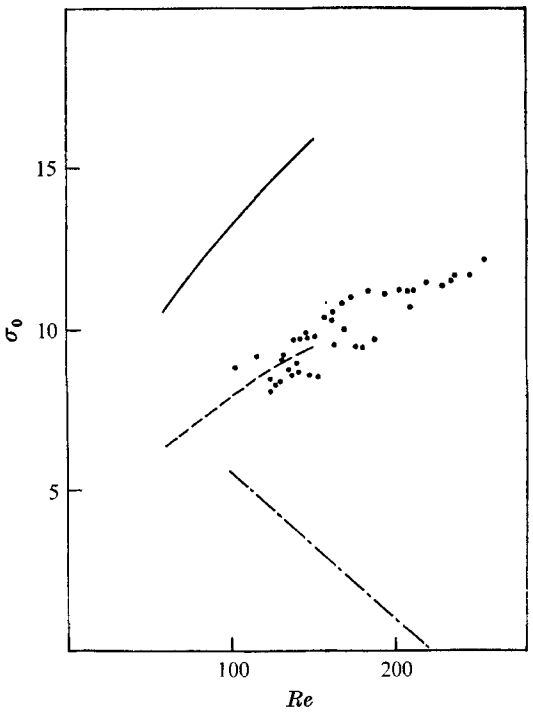

FIGURE 15. Centre frequency of wave peak in units of the table frequency *vs.* Reynolds number for numerous runs at various r and Ω. ——, Lilly most unstable mode (type II); – – –, 60 % of Lilly most unstable mode (type II); —·—, most unstable mode (type I).

were applicable, the calculation of the growth of the waves would require following their progress through from the first Reynolds number at which they become unstable to the Reynolds number at which they are observed. The largest amplitude wave at a particular Reynolds number is not necessarily the one which has the highest growth rate for that Reynolds number, but the one which has grown the most through its entire history. It should be remembered that we have no information as to the direction of propagation of the waves.

Despite the uncertainties involved in comparing observed spectra with growth rates calculated from perturbation theory, it is clear that we are mainly observing type II waves because: (i) The critical Reynolds number, when corrected for curvature (Rossby number) effects, is very close to previous results for type II.

(ii) The central frequencies of the waves are increasing with increasing Reynolds number as in Lilly's calculation for type II, rather than decreasing toward zero as his calculation shows for type I. (iii) The variation of wave intensity with distance from the boundary (figure 14) is consistent with the eigenfunctions shown for type II by Lilly (his figure 12). However, the difference in this respect between types I and II is small.

We are evidently seeing the waves emerge from the general level of disturbances in the flow after they have been growing for some time. At a given frequency, we are seeing waves with many different wavelengths and directions, some of which may in fact be of 'type I'. The distinction becomes somewhat blurred at the higher Reynolds numbers; growth rates vary by no more than a factor of two along a line of constant frequency in figure 16 between the most unstable modes of each sort.

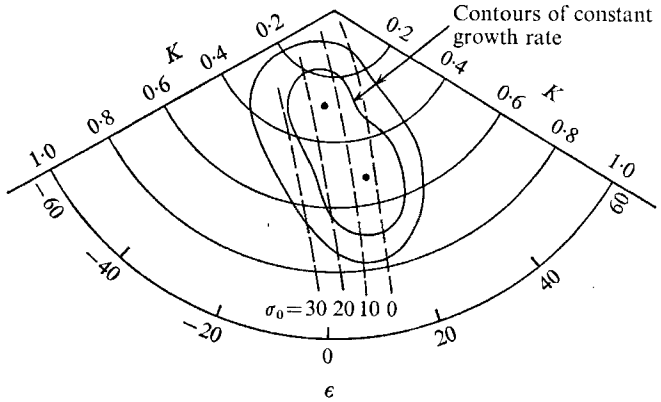

FIGURE 16. Diagram showing the growth rates and frequencies predicted by Lilly for a Reynolds number of 150. (Rossby number is assumed zero.) ●, maxima in growth rate.

The waves observed by Tatro & Mollo-Christensen seemed to have higher Q's, as their chart recordings do not show the 'modulation' characteristics of narrow-band signals, as do those exhibited in our figures 8 and 9.

7. Conclusions

(i) Flows with profiles very closely resembling the idealized Ekman form can be realized in the laboratory. The form of the velocity profiles in the boundary layer is quite close to the Ekman form for Reynolds numbers below 'critical,' and the boundary layer thicknesses are independent of Reynolds number or radial position in this Reynolds number range.

(ii) The 'centrifugal' instabilities mentioned by Faller are associated with a violation of the Rayleigh criterion for stability in this type of apparatus; the Rayleigh criterion predicts the radius beyond which the fluid is unstable.

(iii) Faller's explanation for the apparent variation of critical Reynolds number with Rossby number is confirmed: the fact that the perturbations are carried into regions of higher Reynolds number as they develop, rather than remaining under the same conditions, as in the Couette or Rayleigh–Bénard situations, produces this effect.

(iv) The type II (class A) waves have the spectral characteristics of rather narrow-band signals: the Q of the peak in the power spectrum is between 4 and 5, and does not vary with Reynolds number.

(v) The vertical variations of the power in the wave peak in the spectra resembles the analytical waveforms derived by Lilly. The minimum in the wave energy was found at $z/D = 3{\cdot}5$, while Lilly predicts a minimum at $z/D = 2{\cdot}9$.

(vi) The frequency of the wave peak varies in a manner very similar to that predicted by Lilly for type II (class A) waves, but is only 60 % as great in our apparatus (see figure 15).

(vii) The turbulence had a definite point of onset at a Reynolds number of 150. Its intensity increases quite rapidly as the Reynolds number is increased, growing intense enough to obscure the wave peak when a Reynolds number of 300 is reached. This conclusion may be peculiar to this particular apparatus: in reviewing this paper Faller comments that he has been able to suppress turbulence up to $Re = 500$ (at high Rossby numbers, with careful control of inlet conditions).

This work was carried out at the Institute of Geophysics and Planetary Physics in La Jolla, and was supported principally by NSF Grant GA 849. One of us (C.V.A.) was also partially supported under Project THEMIS Contract No. F44620-68-C-0010.

REFERENCES

FALLER, A. J. 1963 *J. Fluid Mech.* **15**, 560–576.

FALLER, A. J. & KAYLOR, R. E. 1965 *Dynamics of Fluids and Plasmas* (ed. S. I. Paid), 309–320. New York: Academic.

FALLER, A. J. & KAYLOR, R. E. 1966 *J. Atmos. Sci.* **23**, 466–480.

GREENSPAN, H. P. 1968 *The Theory of Rotating Fluids.* Cambridge University Press.

HAUBRICH, R. 1965 *J. Geop. Res.* **70**, 1415–1427.

LILLY, D. K. 1966 *J. Atmos. Sci.* **23**, 481–494.

TATRO, P. R. & MOLLO-CHRISTENSEN, E. L. 1967 *J. Fluid Mech.* **28**, 531–544.